PCCP

Cite this: *Phys. Chem. Chem. Phys.*, 2012, **14**, 10266–10270

www.rsc.org/pccp

PAPER

The structure of 5-cyanoindole in the ground and the lowest electronically excited singlet states, deduced from rotationally resolved electronic spectroscopy and *ab initio* theory†

Olivia Oeltermann,[a] Christian Brand,[a] Bernd Engels,[b] Jörg Tatchen[c] and Michael Schmitt*[a]

Received 5th April 2012, Accepted 18th May 2012
DOI: 10.1039/c2cp41094j

The structure and electronic properties of the electronic ground and the lowest excited singlet states of 5-cyanoindole (5CI) were determined using rotationally resolved spectroscopy of the vibrationless electronic origin of 5CI. In contrast to most other indole derivatives, the lowest excited state of 5CI is determined to be of L_a character. The conventional approximate coupled cluster singles and doubles model (CC2) fails to describe the geometry of the excited state correctly. Nevertheless, scaling the spin components of equal and opposite spins within the CC2 model as proposed by Hellweg *et al.* (*Phys. Chem. Chem. Phys.*, 2008, **10**, 1159) resulted in very good geometry parameters for the excited state.

1 Introduction

Excited singlet states of indole and substituted indoles have found considerable interest due to their potential use as fluorescence probes in proteins. Quantum chemical calculations,[1] two-photon-induced fluorescence anisotropy measurements,[2] two-photon excitation spectroscopy,[3] linear dichroism measurements on partially oriented indole in stretched polyethylene films[4] and rotationally resolved spectroscopy of vibronic bands of indole[5,6] agree that the lowest electronically excited singlet state of indole is the L_b state, energetically followed by the L_a state 1400 cm^{-1} higher in energy.

The introduction of substituents may alter this energetic separation of the two states. Recently we investigated 5-methoxyindole exhibiting the largest known energy gap between L_a and L_b.[7] While DFT/MRCI calculations showed that the L_a was shifted only by 200 cm^{-1} to higher energies, the L_b is stabilized by more than 2000 cm^{-1} relative to indole, attributed to the electron-donating properties of the methoxy group. Hence exchanging the methoxy group for an electron-withdrawing substituent like a cyano group might diminish the L_a–L_b gap considerably and even lead to a reversed state order, having the L_a as the lowest excited singlet state in gas phase. This has been observed so far only for the prominent example of tetrahydrocarbazole.[8] For 2,3-dimethylindole there has been a long lasting debate about the energetic order which was finally resolved by the Callis group by showing that slightest perturbations like an argon matrix as local surrounding shift the L_a origin below the L_b, with a reversed order in gas phase.[9–11]

5-Cyanoindole (5CI) has found some spectroscopic interest as an IR marker probing the local surrounding in proteins.[12] Interestingly, the line width of the CN stretching vibration depends on the solvation of the chromophore. This was also observed by Waegele *et al.* for the appropriate non-natural amino acid 5-cyanotryptophan.[13] The authors analyzed the spectral signature of the CN stretch vibration in H_2O, THF and mixtures thereof, and tested the applicability to the antimicrobial peptide indolicidin. Although 5-cyanotryptophan in a peptide is only a weak fluorophore, it is supposed to be a perfect FRET acceptor from cyanophenylalanine.

In gas phase the spectral position and lifetime of the electronic origin of 5CI were determined by Huang and Sulkes using time-correlated single photon counting for S_1 levels in supersonic free jet expansions.[14]

2 Techniques

2.1 Experimental procedures

5CI ($\geq$ 98%) was purchased from Activate Scientific and used without further purification. The experimental set-up for the rotationally resolved laser induced fluorescence is described in detail elsewhere.[15] In brief, the laser system consists of a single frequency ring dye laser (Sirah Matisse DS) operated with rhodamine 6G, pumped with 7 W of the 514 nm line of a Ar^+-ion laser (Coherent, Sabre 15 DBW). The dye laser

[a] *Heinrich-Heine-Universität, Institut für Physikalische Chemie I, D-40225 Düsseldorf, Germany. E-mail: mschmitt@uni-duesseldorf.de*
[b] *Julius-Maximilians-Universität, Institut für Physikalische und Theoretische Chemie, 97074 Würzburg, Germany*
[c] *Heinrich-Heine-Universität, Institut für Theoretische Chemie, D-40225 Düsseldorf, Germany*

† Electronic supplementary information (ESI) available. See DOI: 10.1039/c2cp41094j

output was coupled to an external folded ring cavity (Spectra Physics Wavetrain) for second harmonic generation. The resulting output power was constant at about 25 mW during the experiment. The molecular beam was formed by co-expanding 5CI, heated to 190 °C, and 400 mbar of argon through a 200 μm nozzle into a vacuum chamber. The molecular beam machine consists of three differentially pumped vacuum chambers that are linearly connected by skimmers (1 mm and 3 mm, respectively) in order to reduce the Doppler width. The resulting resolution is 18 MHz (FWHM) in this set-up. In the third chamber, 360 mm downstream of the nozzle, the molecular beam crosses the laser beam at a right angle. The imaging optics setup consists of a concave mirror and two plano-convex lenses to focus the resulting fluorescence onto a photomultiplier tube, which is mounted perpendicularly to the plane defined by the laser and molecular beam. The signal output was then discriminated and digitized by a photon counter and transmitted to a PC for data recording and processing. The relative frequency was determined with a *quasi* confocal Fabry–Perot interferometer. The absolute frequency was obtained by comparing the recorded spectrum to the tabulated lines in the iodine absorption spectrum.[16]

2.2 Computational methods

2.2.1 Quantum chemical calculations. Structure optimizations were performed employing Dunning's correlation consistent polarized valence triple zeta (cc-pVTZ) basis sets from the Turbomole library.[17,18] The equilibrium geometries of the electronic ground and the lowest excited singlet states were optimized using the approximate coupled cluster singles and doubles model (CC2) employing the resolution-of-the-identity approximation (RI).[19–21] Spin-component scaling (SCS) and scaled opposite-spin (SOS) modifications to CC2 were taken into account.[22] Additionally, we used density functional theory for a restricted closed shell KS determinant using the B3-LYP density functional.[23,24] In these cases, the geometries of the electronically excited singlet states were optimized by means of a time-dependent density functional theory (TDDFT) gradient.[25] All CC2, DFT, and TDDFT calculations were carried out utilizing the Turbomole package, version 6.1.[26] Vibrational frequencies and zero-point corrections to the adiabatic excitation energies have been obtained from numerical second derivatives using the NumForce script.[26] A natural population analysis (NPA)[27] has been performed at the SCS-CC2 optimized geometries using the wavefunctions from the SCS-CC2 calculations as implemented in the Turbomole package.[26]

2.2.2 Fits of the rovibronic spectra using evolutionary algorithms. The search algorithm employed to fit the rotationally resolved electronic spectra is an evolutionary strategy adapting normal mutations *via* a covariance matrix adaptation (CMA-ES) mechanism. This algorithm was developed by Ostermeier and Hansen *et al.*[28,29] and is designed especially for optimization on rugged search landscapes that are additionally complicated due to noise, local minima and/or sharp bends. It belongs, like other search algorithms we also use, to the group of global optimizers that were inspired by natural evolution. For a detailed description of this evolutionary strategy we refer to ref. 7 and 30.

3 Results

3.1 High resolution spectrum of the origin band of 5-cyanoindole

Fig. 1 shows the rotationally resolved spectrum of the electronic origin of 5CI at 33 874 cm^{-1}. The experimental spectrum could be simulated with a rigid rotor Hamiltonian and almost pure a-type selection rules (the angle θ in Table 1 is practically zero). The enlarged portion of the spectrum shows the excellent agreement between experiment and simulation using the parameters from the best fit employing the CMA-ES strategy. The fit of the line shapes to Voigt profiles using a Gaussian (Doppler) contribution of 18 MHz yielded a Lorentzian contribution of 13 ± 2 MHz to the total line width equivalent to an excited state life time of 12 ± 2 ns, in fair agreement with the value from time-resolved spectroscopy of 16.9 ns by Huang and Sulkes.[14]

We additionally tried a different Hamiltonian in the fit of the spectrum, containing axis reorientation effects.[31] This Hamiltonian improved the fit of the intensities in the spectrum

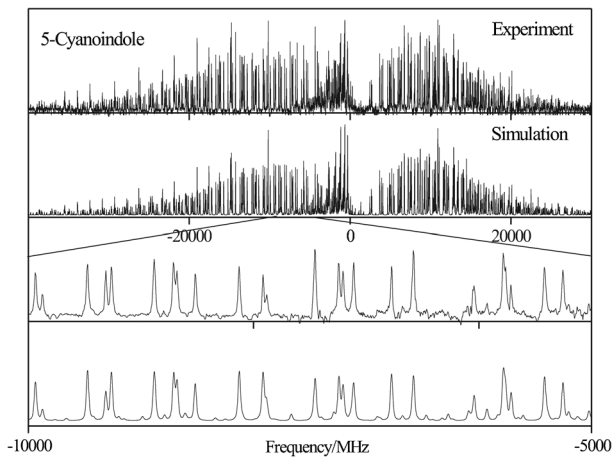

Fig. 1 Rotationally resolved electronic spectrum of the electronic origin of 5-cyanoindole.

Table 1 CC2 and (TD)DFT calculated molecular parameters of 5-cyanoindole. Changes of the rotational constants are defined as: $\Delta B_g = B'_g - B''_g$, with B_g as rotational constants with respect to the inertial axes $g = a, b, c$. ν_0 is the center frequency of the band, and f the oscillator strength

	DFT[b]	CC2[a]	SCS-CC2[a]	SOS-CC2[a]	Exp.
A''/MHz	3387	3368	3364	3361	3370.4(16)
B''/MHz	740	736	734	732	738.00(2)
C''/MHz	607	604	602	601	605.93(1)
$\Delta I''$/amu Å^2	0.0	0.0	0.0	0.0	−0.1385
A'/MHz	3436	3379	3281	3269	3299.9(16)
B'/MHz	723	720	725	725	730.32(3)
C'/MHz	597	594	594	594	598.16(2)
$\Delta I'$/amu Å^2	0.0	0.0	0.0	0.0	−0.2582
ΔA/MHz	+49	+11	−83	−92	−70.47(1)
ΔB/MHz	−17	−16	−9	−7	−7.69(1)
ΔC/MHz	−10	−10	−6	−7	−7.37(1)
θ/°	26.0	51.8	9.4	9.5	3(3)
ν_0/cm^{-1}	33 930	34 947	34 758	34 466	33 874
f	0.03	0.03	0.01	0.01	—

[a] CC2 calculations have been performed with the cc-pVTZ basis set. [b] (TD)DFT calculations have been performed with the B3-LYP functional with the cc-pVTZ basis set.

of indole considerably.[6] In 5CI no similar improvement was observed, imposing an upper limit of 0.2° on the axis reorientation angle θ_T. Different thermalization of different JK_AK_c states in the molecular beam requires a description of populations using several temperatures, which take the different rotational cooling into account. We used the two temperature model, proposed by Wu and Levy[32] with $n_i = e^{-E_i/kT_1} + we^{-E_i/kT_2}$, where n_i is the population of the ith rovibronic level at energy E_i, k is the Boltzmann constant, T_1 and T_2 are the two temperatures, and w is a weighting factor modelling the contribution from T_2. The best agreement between experimental and simulated spectra could be obtained with $T_1 = 2.2$ K, $T_2 = 4.5$ K and $w = 0.1$.

3.2 Computational results

Table 1 collects the structural data (*i.e.* rotational constants (A, B, and C)) in the electronic ground (double prime) and excited (single prime) states, their changes upon electronic excitation (ΔA, ΔB, and ΔC), and the respective inertial defects.‡ All equilibrium structures, optimized at the DFT, CC2, SCS-CC2, or SOS-CC2 level of theory without imposing symmetry constraints, are perfectly planar. Their calculated inertial defects are exactly zero. The experimental value contains vibrational corrections from the vibrational averaging of the ground and excited state structures. The difference of the experimental and the calculated ΔI values gives a first order approximation to the amount of vibrational averaging contained in the experimental rotational constants. We estimate the vibrational contributions to the equilibrium rotational constants to be less than 0.1% *i.e.* a maximum of 3 MHz absolutely.

Obviously, the DFT calculations yield wrong structures for the lowest electronically excited state, here. Instead of the large reduction of the rotational constant A that has been found in the experiment, even a considerable increase in A of 49 MHz is obtained. Genuine CC2 does slightly better, but still gives the wrong sign for A upon electronic excitation. In contrast, SCS-CC2 and SOS-CC2 yield the rotational constants in the lowest electronically excited state, as well as their changes upon excitation with respect to the ground state constants, correctly. Similar improvements with SCS-CC2 were recently also found for paracyclophane systems.[33]

In the following we will compare the relevant bond lengths of the different calculations directly. Table 2 gives the bond lengths of 5CI in the electronic ground and lowest excited singlet states from CC2, SCS-CC2, and SOS-CC2 calculations utilizing the cc-pVTZ basis set. Genuine CC2 failed to localize the S_2 state. For atomic numbering *cf.* Fig. 2. According to both SCS-CC2 and SOS-CC2, the main geometry changes upon electronic excitation to the S_1 state take place in the benzene ring, while the pyrrole ring is subject only to minor changes. In addition, the C5C10 bond length decreases, while the C10N11 bond in the cyano group gets moderately elongated. These bond length changes are in line with a quinoidal type structure in the excited state, shown in Fig. 2c and d.

‡ The inertial defect is a measure of the non-planarity of a molecule in a given electronic state, and is defined as: $\Delta I = I_C - I_A - I_B$. For a planar molecule it is close to zero.

Table 2 Bond lengths of 5CI in the electronic ground and lowest excited singlet states from CC2, SCS-CC2, and SOS-CC2 calculations utilizing the cc-pVTZ basis set. For atomic numbering *cf.* Fig. 2

State	S_0			S_1			S_2	
Method	CC2	SCS-CC2	SOS-CC2	CC2	SCS-CC2	SOS-CC2	SCS-CC2	SOS-CC2
N1C2	138.0	138.3	138.5	133.5	138.3	138.9	136.6	136.2
C2C3	137.5	137.3	137.2	142.9	139.4	138.9	142.0	142.6
C3C9	142.9	143.5	143.8	140.5	141.4	141.9	143.5	143.1
C9C4	140.0	140.3	140.4	141.9	141.9	141.9	141.5	141.6
C4C5	139.5	139.4	139.4	144.6	144.2	144.4	145.1	145.1
C5C6	141.6	141.8	142.0	143.3	144.8	144.6	138.7	138.7
C6C7	138.6	138.6	138.5	140.9	142.0	142.3	144.0	144.4
C7C8	139.8	140.1	140.3	140.9	140.7	140.9	139.4	139.2
C8C9	142.5	142.2	142.0	142.5	146.2	146.4	142.1	142.5
C8N1	137.2	137.5	137.6	141.7	138.1	137.8	139.4	139.7
N1H12	100.6	100.5	100.4	100.9	100.5	100.5	101.2	101.2
C5C10	143.0	143.7	144.0	140.8	141.6	142.1	143.0	143.4
C10N11	118.2	117.6	117.4	119.0	118.2	117.9	117.9	117.6

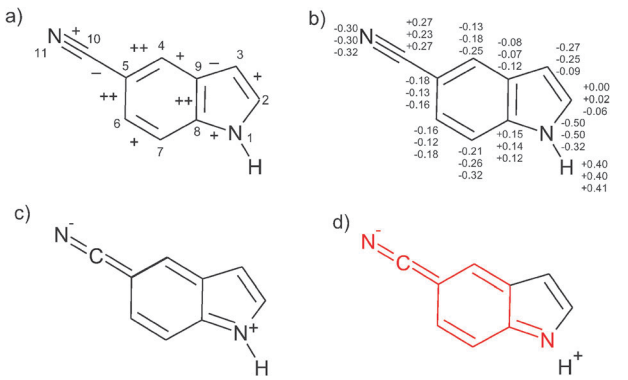

Fig. 2 (a) Atomic numbering and changes of the bond lengths upon electronic excitation to the lowest excited singlet state in 5CI from the SCS-CC2 calculations. A + sign along with a bond represents a small increase in the bond length, + + a large one, similarly decreases are indicated by − signs. A missing symbol means no or tiny bond length changes. (b) Natural charges of the S_0, S_1 and S_2 states (numbers at each atom from top to bottom) from a natural bond orbital analysis. (c) and (d) Possible mesomeric resonance structures of 5CI. In the second mesomeric structure, the structural motif of p-aminobenzonitrile is marked in red.

In contrast, the genuine CC2 method also predicts pronounced changes within the pyrrole moiety: according to Table 2, the CC2 S_1 geometry exhibits strong elongations of the C8N1 and C2C3 bonds, whereas N1C2 is shorter than in the S_0 ground state. Comparison of these geometry changes to the ones obtained from SCS-CC2 and SOS-CC2 optimizations of the S_2 state shows that obviously the S_1 and S_2 states change their energetic order in the CC2 calculations.

The direction of the transition dipole moment (TDM) in the molecular frame is an important indicator of the electronic nature of the excited state. For a planar molecule its orientations with respect to the inertial a and b-axes are defined *via* the angle θ, which is the angle of the transition moment vector with the molecule fixed a-axis:

$$\mu_a = \mu\cos\theta \text{ and } \mu_b = \mu\sin\theta$$

The squares of the projections onto the inertial axes are directly proportional to the experimentally observed contribution to the

Table 3 SCS-CC2 calculated properties of the ground and lowest two electronically excited states of 5CI at their respective minimum geometries

State	S_0	S_1	S_2
	—	+0.56 (H → L)	0.77 (H → L)
Main	—	−0.51 (H − 1 → L)	+0.44 (H − 1 → L)
contributions	—	+0.44 (H − 1 → L+1)	−0.29 (H → L + 1)
	—	+0.42 (H → L + 1)	−0.26 (H − 2 → L)
ν_0/cm^{-1}	—	34 811	37 002
f	—	0.01	0.03
θ/°	—	9.4	65.1
μ/D	7.1	8.1	10.1
θ_D/°	15.8	12.9	3.0

band type in the electronic absorption spectrum. Only SCS-CC2 and SOS-CC2 calculations yield comparably small values of θ for the S_1 state as observed in experiment. In contrast, the direction of the S_1 transition dipole moment (θ = 51.8°) as predicted by genuine CC2 is clearly qualitatively wrong. Employing the SCS-CC2 approach, a similarly large value is obtained for the S_2 state (*cf.* Table 3). This finding corroborates the above view that CC2 predicts an adiabatically wrong order of states. The B3-LYP value for θ is situated approximately half way between those of S_1 and S_2 as predicted by SCS-CC2. We thus conclude that the lowest electronically excited state has the TDM orientation along the *a*-axis, while the second singlet state is an *ab*-hybrid, with predominantly *b*-type (Fig. 3).

Inspection of the leading contributions of the configurations to the excited states as calculated with SCS-CC2 shows that the adiabatically lowest S_1 state is characterized by 0.56 (HOMO → LUMO) − 0.51 (HOMO − 1 → LUMO) + 0.44 (HOMO − 1 → LUMO + 1) + 0.42 (HOMO → LUMO + 1) excitation (*cf.* Fig. 4). The S_2-state is comprised of 0.77 (HOMO → LUMO) + 0.44 (HOMO − 1 → LUMO) − 0.29 (HOMO → LUMO + 1) − 0.26 (HOMO − 2 → LUMO). The excitation to both states is therefore heavily mixed and the second excited singlet state is accompanied by a considerable charge migration from the indolic NH group to the cyano group.

Table 3 collects the properties of the ground and lowest two excited singlet states of 5CI, calculated at their respective minimum geometries. Given are the main contributions to the excited states, the oscillator strengths *f*, the transition dipole moment orientations θ with respect to the inertial *a*-axis, the adiabatic excitation energies ν_0/cm^{-1}, and the permanent dipole moments μ. 5CI has a very high dipole moment of 7.1 D already in the electronic ground state, resulting from the push–pull properties of the NH/CN groups. In the S_1 state the dipole moment increases moderately to 8.1 D, while for the S_2 state a large permanent dipole of 10.1 D is calculated. For this state, the permanent dipole moment is oriented nearly exactly along the inertial *a*-axis (*cf.* angle θ_D in Table 3), while the dipole moment of the S_1 state is tilted by 13° with respect to the *a*-axis and that of the ground state is rotated by 16°.

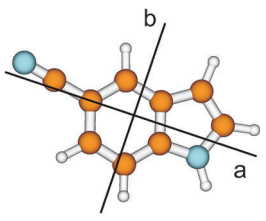

Fig. 3 Orientation of the inertial axes in 5CI.

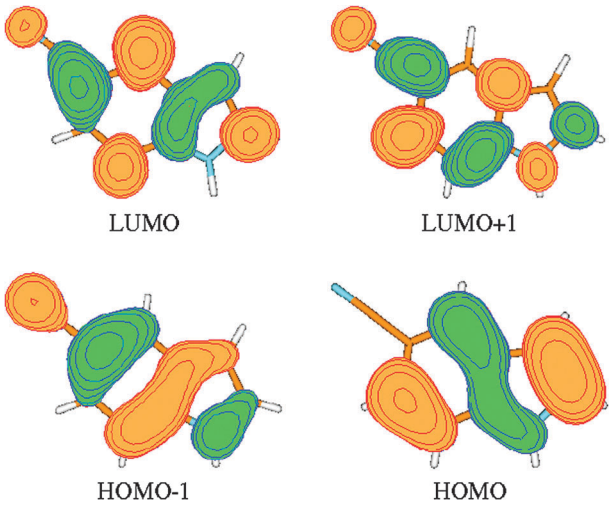

Fig. 4 Contour plots of the highest occupied and lowest unoccupied molecular orbitals of 5CI at the optimized S_1 geometry from SCS-CC2/cc-pVTZ calculations, isosurface value 0.03.

The zero-point corrected adiabatic excitation energies (ν_0) of the lowest two excited singlet states are given in Table 3. For the SCS-CC2 calculations, the calculated value of 34 811 cm^{-1} is in good agreement with the experimental value (33 874 cm^{-1}). The energetically following state has a calculated adiabatic excitation energy of 37 002 cm^{-1}.

4 Discussion

From the comparison of experimental and theoretical rotational constants of 5CI we have found that the structure in the electronic ground state can reasonably be reproduced at the DFT/cc-pVTZ and the CC2/cc-pVTZ levels of theory. Nevertheless, for the lowest two excited states, serious problems regarding the structure and the transition dipole moment orientation are encountered using TD-DFT and CC2, since both methods change the energetic order of the lowest two excited singlet states. This is very surprising at first sight, since the S_1 structures of comparable molecules (indole, 5-methoxyindole, tetrahydrocarbazole) have been computed using CC2 without any difficulties. The main difference between 5-cyanoindole and the before mentioned indoles is the fact that the cyano group facilitates a charge migration from the indolic NH moiety to the cyano group through the strong negative mesomeric (−M) effect of this group. Similar effects are observed for the charge transfer (CT) state of dimethylaminobenzonitrile (DMABN), which shows a twisted intramolecular charge transfer (TICT) conformation in its S_2 state, for a review see *e.g.* ref. 34. In 5CI the S_1 state is clearly a locally excited (LE) state, while for the S_2 state some CT character can be discussed. Inspection of the natural charges from a NBO analysis shows that the electron density at N1 remains constant upon excitation to the S_1 state, but is greatly reduced upon excitation to S_2. Similarly, the negative charge at C3 decreases in the S_2 state, while the negative charges at C4 and

C7 increase, as shown in Fig. 2. The corresponding isosurface plots of the density change for both excitations as calculated with the SCS-CC2 method can be found in Fig. S1 of the ESI.†

The main difference between 5CI and DMABN lies in the conformational rigidity of 5CI. The C2–C3 bond bridges the amino position, forcing the amino group into planarity. Thus, the conical intersection, which is discussed for DMABN *via* the twisting mode that connects the primarily excited planar CT state with the LE state, does not exist in 5CI.

It is well-known that many DFT functionals, among them common generalized gradient approximation and hybrid functionals, often fail to describe CT states correctly.[35,36] Nevertheless, the S_1 state structure, we predict using TD-DFT, is not completely off. This could result since the size of the TD-DFT error correlates with the spatial overlap in a given excitation[37] which for the present case does not vanish at all.

The larger importance of electron correlation effects in the excited state is reflected in the rather poor description of the excited state structure using the plain CC2 model. Hellweg *et al.* stated that "spin-component scaling makes the CC2 model somewhat more robust against strong correlation effects; in particular for systems with triple bonds".[22] For 5CI in the ground state, correlation effects which can be traced back to the electrons in the CN triple bond may play a minor role compared to electronic effects of the chromophore. Upon electronic excitation to the lowest singlet state, electron density from the pyrrolic NH group is shifted to the chromophore. This additional electron density is most efficiently delocalized aided by the cyano group. Thus, correlation of the electrons in the CN triple bond does play a major role in the electronically excited state.

5 Conclusions

The ground and excited state rotational constants of 5-cyano-indole could be determined by analysis of the rotationally resolved electronic spectrum and were compared to those from *ab initio* calculated structures. A good agreement for both electronic states involved in the transition could be obtained using spin component scaled CC2 calculations, while plain CC2 failed to describe the excited state structure correctly. From the analysis of the transition dipole moment orientation in the molecular frame, the nature of the lowest electronically excited state has been determined to be L_a like in the nomenclature of Platt. It is mainly an LE state, while for the S_2 state some CT character can be discussed from the results of the SCS-CC2 calculations.

Acknowledgements

This work was financially supported by the Deutsche Forschungsgemeinschaft SCHM1043/11-1(M. S.) and the Research Training School GRK 1221 (B. E.). J. T. also acknowledges support by the Deutsche Forschungsgemeinschaft DFG, project reference TA725/1-1.

References

1 P. R. Callis, *J. Chem. Phys.*, 1991, **95**, 4230.
2 P. R. Callis, in *Topics in Fluorescence Spectroscopy*, ed. J. Lakowicz, Plenum Press, New York, 1977, vol. 5, pp. 1–42.
3 D. M. Sammeth, S. Yan, L. H. Spangler and P. R. Callis, *J. Phys. Chem.*, 1990, **94**, 7340.
4 B. Albinsson and B. Nordén, *J. Phys. Chem.*, 1992, **96**, 6204.
5 C. Brand, J. Küpper, D. W. Pratt, W. L. Meerts, D. Krügler, J. Tatchen and M. Schmitt, *Phys. Chem. Chem. Phys.*, 2010, **12**, 4968–4997.
6 J. Küpper, D. W. Pratt, W. L. Meerts, C. Brand, J. Tatchen and M. Schmitt, *Phys. Chem. Chem. Phys.*, 2010, **12**, 4980–4988.
7 C. Brand, O. Oeltermann, D. W. Pratt, R. Weinkauf, W. L. Meerts, W. van der Zande, K. Kleinermanns and M. Schmitt, *J. Chem. Phys.*, 2010, **133**, 024303.
8 O. Oeltermann, C. Brand, W. L. Meerts, J. Tatchen and M. Schmitt, *J. Mol. Struct.*, 2011, **933**, 2–8.
9 K. W. Short and P. R. Callis, *Chem. Phys.*, 2002, **283**, 269.
10 B. Fender and P. R. Callis, *Chem. Phys. Lett.*, 1996, **262**, 343–348.
11 A. A. Rehms and P. R. Callis, *Chem. Phys. Lett.*, 1987, **140**, 83.
12 M. M. Waegele and F. Gai, *J. Phys. Chem. Lett.*, 2010, **1**, 781–786.
13 M. M. Waegele, M. J. Tucker and F. Gai, *Chem. Phys. Lett.*, 2009, **478**, 249–253.
14 Y. Huang and M. Sulkes, *Chem. Phys. Lett.*, 1996, **254**, 242–248.
15 M. Schmitt, J. Küpper, D. Spangenberg and A. Westphal, *Chem. Phys.*, 2000, **254**, 349–361.
16 S. Gerstenkorn and P. Luc, *Atlas du spectre d'absorption de la molécule d'iode*, CNRS, Paris, 1982.
17 R. Ahlrichs, M. Bär, M. Häser, H. Horn and C. Kölmel, *Chem. Phys. Lett.*, 1989, **162**, 165–169.
18 J. T. H. Dunning, *J. Chem. Phys.*, 1989, **90**, 1007.
19 C. Hättig and F. Weigend, *J. Chem. Phys.*, 2000, **113**, 5154–5161.
20 C. Hättig and A. Köhn, *J. Chem. Phys.*, 2002, **117**, 6939–6951.
21 C. Hättig, *J. Chem. Phys.*, 2002, **118**, 7751–7761.
22 A. Hellweg, S. Grün and C. Hättig, *Phys. Chem. Chem. Phys.*, 2008, **10**, 4119–4127.
23 P. J. Stephens, F. J. Devlin, C. F. Chabalowski and M. J. Frisch, *J. Phys. Chem.*, 1994, **98**, 11623–11627.
24 C. Lee, W. Yang and R. Parr, *Phys. Rev. B: Condens. Matter Mater. Phys.*, 1988, **37**, 785–789.
25 F. Furche and R. Ahlrichs, *J. Chem. Phys.*, 2003, **117**, 7433.
26 TURBOMOLE V6.1 2009, a development of University of Karlsruhe and Forschungszentrum Karlsruhe GmbH, 1989–2007, TURBOMOLE GmbH, since 2007, available from http://www.turbomole.com.
27 A. E. Reed, R. B. Weinstock and F. Weinhold, *J. Chem. Phys.*, 1985, **83**, 735–746.
28 A. Ostermeier, A. Gawelczyk and N. Hansen, Lecture Notes in Computer Science: Parallel Problem Solving from Nature (PPSN III), Springer, 1994, pp. 189–198.
29 N. Hansen and A. Ostermeier, *Evol. Comput.*, 2001, **9**, 159–195.
30 W. L. Meerts and M. Schmitt, *Int. Rev. Phys. Chem.*, 2006, **25**, 353–406.
31 A. Held, B. B. Champagne and D. W. Pratt, *J. Chem. Phys.*, 1991, **95**, 8732.
32 Y. R. Wu and D. H. Levy, *J. Chem. Phys.*, 1989, **91**, 5278–5284.
33 C. Schon, W. Roth, I. Fischer, J. Pfister, C. Kaiser, R. F. Fink and B. Engels, *Phys. Chem. Chem. Phys.*, 2010, **12**, 9339–9346.
34 Z. R. Grabowski, K. Rotkiewicz and W. Rettig, *Chem. Rev.*, 2003, **103**, 3899.
35 A. Dreuw, J. L. Weisman and M. Head-Gordon, *J. Chem. Phys.*, 2003, **119**, 2943.
36 H.-M. Zhao, J. Pfister, V. Settels, M. Renz, M. Kaupp, V. C. Dehm, F. Würthner, R. F. Fink and B. Engels, *J. Am. Chem. Soc.*, 2009, **131**, 15660–15668.
37 M. J. G. Peach, P. Benfield, T. Helgaker and D. J. Tozer, *J. Chem. Phys.*, 2008, **128**, 044118.

